Wideband Interferometry in Synthetic Aperture Sonar

Torstein Olsmo Sæbø, *Member, IEEE*, Stig Asle Vaksvik Synnes, and Roy Edgar Hansen, *Member, IEEE*

***Abstract*—Synthetic aperture sonar (SAS) interferometry can provide very high resolution images and topographic maps of the seafloor over large swaths. Processing of interferometric data to retrieve reliable depth estimates of the seafloor is, however, non-trivial. Traditional narrowband interferometry processing relies on advanced phase unwrapping techniques, constraints, and prior knowledge to resolve phase ambiguities. These methods all have dependence throughout the dataset, e.g. a small error in the assumption may cause a global error in the final phase estimate. For wideband systems there are alternative techniques to estimate the absolute (or ambiguity-free) phase difference directly. We consider four different wideband interferometry techniques for direct phase difference estimation: complex cross correlation, split-spectrum algorithm, and the multi-chromatic approach. In addition, we develop a weighted split-spectrum algorithm, where the weights minimizes the variance in the absolute phase estimate. We benchmark these techniques on simulated data and demonstrate the techniques on real data from the HISAS wideband interferometric SAS on a HUGIN autonomous underwater vehicle. We have found the following: The cross correlation technique always outperforms the other techniques in misregistrated areas caused by severe topographic changes. The split spectrum techniques are substantially faster than the cross correlation technique. The multi-chromatic approach has similar performance as the multiband split spectrum technique for the same choice of bands. We demonstrate that all the wideband interferometry techniques outperform a standard Goldstein's Branch cut phase unwrapping algorithm on real data from a complicated scene containing an elevated target and severe layover.**

***Index Terms*—Synthetic aperture sonar (SAS), synthetic aperture radar (SAR), wideband interferometry, complex cross correlation, split spectrum algorithm, multi chromatic analysis**

I. Introduction

Interferometry refers to a family of techniques where interference phenomena between waves are used to measure e.g. the shift between two dataset. In synthetic aperture radar (SAR) interferometry means measuring the shift between SAR images. If the sensor positions are separated with a vertical baseline, the across-track shift can be used to estimate the topography.

Synthetic aperture sonar (SAS) technology (similar to SAR) has matured substantially the last few years [1], [2]. As for radar, interferometry has been considered for SAS [3]–[5], with specific differences between SAS and SAR [6], [7].

Manuscript received June 30, 2012; revised later on

The authors are with the Norwegian Defence Research Establishment (FFI), P.O. Box 25, N-2027 Kjeller, Norway.

E-mail: Torstein-Olsmo.Sabo@ffi.no; Stig-Asle.Synnes@ffi.no; Roy-Edgar.Hansen@ffi.no.

Fig. 1. The HUGIN autonomous underwater vehicle equipped with the HISAS wideband interferometric synthetic aperture sonar.

The Norwegian Defence Research Establishment (FFI) and Kongsberg Maritime have a long term collaboration to develop SAS technology. Fig. 1 shows a HUGIN autonomous underwater vehicle (AUV) onboard FFI's research vessel H. U. Sverdrup II. The vehicle is equipped with a HISAS 1030 wideband interferometric SAS with two receiver arrays for single-pass interferometry and 30% relative bandwidth [8], [9].

Traditional SAR interferometry techniques [10]–[12] rely on coregistered images and advanced phase unwrapping techniques to produce Digital Elevation Models (DEM). For wideband systems, the absolute (or ambiguity-free) phase difference between two images can be estimated directly [13]–[15]. In this paper we consider four different techniques: The *complex cross correlation* (CCC) technique used in standard time delay estimation [16], [17]. The *split-spectrum* algorithm (SSA), based on splitting the signal into two frequency subbands and generating an differential interferogram (similar to Delta-k) [18], [19]. The *multi-chromatic approach* (MCA), based on generating multiple interferograms in different frequency bands. The interferograms will wrap at different intervals, and the wraps that minimizes the subband differences are chosen [20], [21]. We have also developed a *weighted multiband split-spectrum* algorithm (WSSA), where multiple bands are formed, and interferograms at all difference frequencies are constructed. The weights are chosen based on the signal to noise ratio and the frequency separations. We study the theoretical performance of these techniques, evaluate their performance on a simulated scenario, and finally apply the methods on real data from the HISAS interferometric SAS.

DOI til publisert versjon / DOI to published version: 10.1109/TGRS.2013.2244900

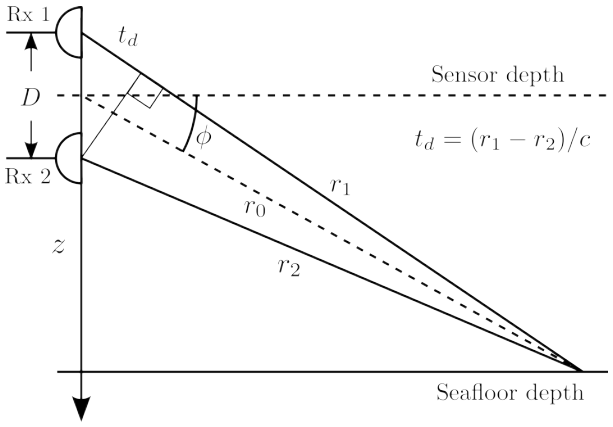

Fig. 2. Geometry of seafloor depth estimation.

In section II we review the basic principle of depth estimation by interferometry, in section III we describe the different techniques for absolute phase difference estimation. In IV we describe the processing flow for wideband interferometry, and in V we assess the performance of the different techniques on simulated data. In VI we show wideband interferometry results on real data collected by HUGIN AUV, and in VII we conclude our work.

II. Depth Estimation

We construct a master SAS image $s_m(t, x)$ and slave SAS image $s_s(t, x)$ from two vertically displaced arrays, where t is the two-way travel time and x is the position along the synthetic aperture. By estimating the time delay, $t_d(t)$, between corresponding image features, we obtain a depth-estimate relative to the sonar coordinate system [10], [22, chapter 5]

$$z(t) = r\frac{c}{D}t_d(t). \tag{1}$$

Here $r = ct/2$ is the one way range, c is the sound speed and D the interferometric baseline (see Fig. 2). The depth estimation is thus reduced to a time delay estimation problem.

A. Coarse co-registration

In order to extract the phase difference (or the corresponding time delay) between the master and slave SAS images, the images must be co-registered [22], [23]. The success of the co-registration can be estimated from the coherence between the two images. Coherence is here defined as the amplitude of the complex degree of coherence [10, chapter 4.3]

$$\gamma(\tau) = \frac{\langle s_m s_s^*(t_d - \tau)\rangle}{\left[\langle |s_m|^2\rangle \langle |s_s|^2\rangle\right]^{1/2}} \tag{2}$$

evaluated at zero-lag, $\tau = 0$. The coherence has the property $0 \leq |\gamma(\tau)| \leq 1$. For simplicity, we have omitted the time- and position arguments.

Registration within a fraction of a resolution cell is required for accurate phase estimation modulo 2π. For absolute (ambiguity free) phase difference estimation, registration to within the wrapping interval is also required. The image resolution along the (two-way) time axis is $1/B$, and the wrapping interval of the phase difference is $1/f_c$, where B is the full bandwidth and f_c the center frequency. This means that, in general, co-registration to within the wrapping interval is only achievable for ultra-wideband systems with high signal-to-noise ratio (SNR). The co-registration is usually performed through a warping function estimated from a set of control points [24], or through an *a priori* knowledge of the seafloor depth [5]. Both the warping function and the *a priori* seafloor depth are typically of too low order to capture rapid depth changes, which occur on complicated objects. This means that in practice, there will always be some occurrence of wrap ambiguities in the phase differences.

B. Interferogram estimation

For each resolution cell in the co-registered SAS images, the complex interferogram γ around the center frequency f_c is computed through

$$\gamma(f_c) = s_m(f_c)s_s^*(f_c). \tag{3}$$

In practice a sliding maximum likelihood phase estimation filter is used to reduce the phase noise in the complex interferogram at the cost of reduced spatial resolution [25, chapter 3.2], [10, chapter 4.3]. The interferometric phase difference, $\psi_w(f_c) = \arg\{\gamma(f_c)\}$, is a function of the interferometric time delay. However, the phase difference is available only modulo 2π, with the absolute phase difference between the two images, $\psi_a(f_c)$, defined as

$$\psi_a(f_c) = 2\pi f_c t_d. \tag{4}$$

The time delay is thus related to the absolute phase difference and the interferometric (wrapped) phase difference through

$$t_d = \frac{\psi_a(f_c)}{2\pi f_c} = \frac{\psi_w(f_c)}{2\pi f_c} + \frac{k(f_c)}{f_c}, \tag{5}$$

where $k(f_c)$ is the number of 2π-wraps at center frequency.

C. Phase unwrapping

A common method used to resolve phase ambiguities in the interferogram is a 2D phase unwrapper [25]. A phase unwrapper assumes that the phase differences between neighboring pixels are less than π. Phase unwrappers therefore add additional information and may outperform absolute phase difference estimators. However, when using 2D phase unwrappers, any small error in the assumption may cause an global error in the final depth estimate, since all pixels are dependent. In this paper we have chosen to use a standard Goldstein's Branch cut algorithm, as described in [25, chapter 4.2], as a benchmark method. There do exist more advanced phase unwrappers, but since our effort in this paper is concentrated in estimating the absolute phase differences directly more advanced phase unwrappers are outside the scope of this article.

Dette er en postprint-versjon / This is a postprint version.
DOI til publisert versjon / DOI to published version: 10.1109/TGRS.2013.2244900

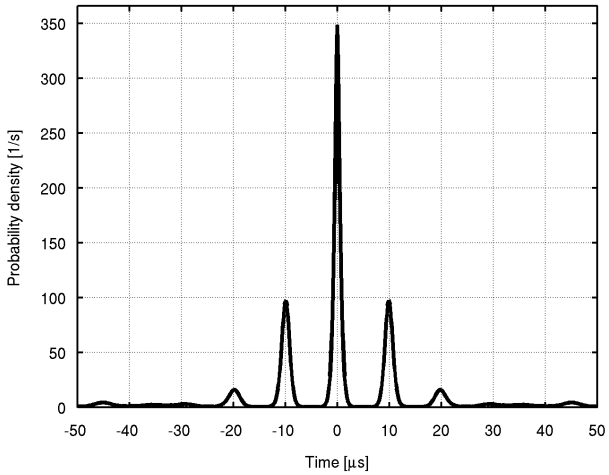

Fig. 3. Approximated probability density function (PDF) for estimation of delay τ with the maximum likelihood estimator. The example is for 0 dB SNR, 100 kHz center frequency, 30% relative bandwidth and 0.5 ms integration time.

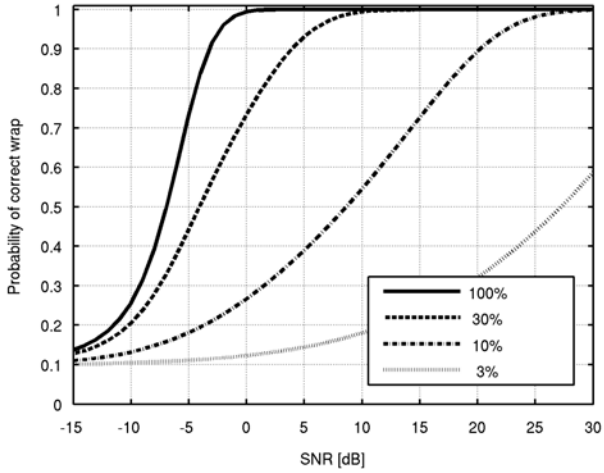

Fig. 4. Theoretical probability of correct wrap as a function of SNR and relative bandwidth. The length of the series is 0.5 ms, corresponding to 50 independent samples for 30% relative bandwidth, and the search is limited within ± 5 wraps.

III. Absolute Phase Difference Estimators

The challenge of absolute phase difference estimation is to obtain the correct wrap. Different absolute phase estimators will have different performance, but a non-adaptive method cannot perform better than the maximum likelihood estimator (MLE). The performance of such an estimator has been studied in detail [26], [27]. The probability of estimating a delay offset τ cannot generally be expressed in a closed analytic form, but a closely approximated expression is given in [27, eq 4-8], assuming a large number of independent samples. The related probability density function (PDF), $p(\tau)$, is a function of the SNR, frequency interval, the length of the time series (i.e. the number of independent samples) and the sensor separation in wavelengths. In Fig. 3 we show $p(\tau)$ for an example case with 0 dB SNR, 100 kHz center frequency, 30% relative bandwidth and 0.5 ms integration time, limited to an interval of ± 5 wraps. We observe that the function describes the lower bound regarding both the probability for incorrect wrap and the accuracy within each wrap.

The probability of obtaining the correct wrap is found by integrating $p(\tau)$ over the interval $[-1/(2f_c), 1/(2f_c)]$. Examples on the maximum theoretical probability of obtaining the correct wrap as a function of SNR and relative bandwidth is presented in Fig. 4. The signal frequency is 100 kHz, and the length of the time series is 0.5 ms, corresponding to 50 independent samples for 30% relative bandwidth. The absolute phase difference error is limited within ± 5 wraps, hence the lower value is 0.1. We see that a wideband system with e.g. 30% relative bandwidth has substantially better probability to estimate correct wrap than a narrowband system. This is an important finding, and suggests that absolute phase techniques can potentially achieve good performance on wideband systems.

In the rest of this section, we describe four different techniques for absolute phase difference estimation.

A. Complex Cross Correlation (CCC)

Peak detection in the complex cross correlation (CCC) of the two sequences is the Maximum Likelihood Estimator for differential shift estimation of partially correlated sequences [22, chapter 5.4], [28]. The MLE has the asymptotic properties of being unbiased and achieving the Cramér-Rao lower bound (CRLB) [29, chapter 7]. The master and slave images must be oversampled before the fine-level (sub-resolution) cross correlation to avoid aliasing [10, chapter 2.5.3], and the step interval for the CCC evaluation should not exceed the ambiguity interval. Then the peak magnitude is detected, and can be used to determine the absolute phase (and thereby the correct wrap interval)

$$\psi_a(f_c) = 2\pi f_c \arg\max_{\tau} |\gamma(\tau)| \tag{6}$$

The ability to estimate correct wrap is dependent on the relative bandwidth and the signal to noise ratio [27], [17]. For systems with limited bandwidth, CCC is less suited as an absolute phase difference estimator. In the limit of ultra-wideband systems, the phase becomes ambiguity free [30], and only phase noise within the wrap interval affects the accuracy of the depth estimation. CCC is computational heavy compared to the other techniques in this paper. It starts from the coarse co-registrated images and performs fine-level (sub-resolution) co-registration over the entire image. CCC also allows for searching outside the initial pixel correlations, and therefore is a more robust method.

In the case of non-white noise and/or non-white signal, standard CCC may not be optimum, and techniques like the generalized cross correlation (GCC) [31], [32] can potentially improve the performance.

B. Split-Spectrum Algorithm (SSA)

The split-spectrum algorithm (SSA) splits the full bandwidth B into two non-overlapping subbands of bandwidth b.

Dette er en postprint-versjon / This is a postprint version.
DOI til publisert versjon / DOI to published version: 10.1109/TGRS.2013.2244900

Then the interferogram from each subband is formed, and thereafter combined into a differential interferogram [19]. By expressing both bands through equation (5), we observe that this corresponds to an interferogram at the differential frequency

$$\psi_a(\Delta f) = 2\pi(f_2 - f_1)t_d = \psi_a(f_2) - \psi_a(f_1) \tag{7}$$

where f_1 and f_2 are the frequencies of each subband and $\Delta f = f_2 - f_1$. The advantage is that this interferogram wraps with the larger period $1/\Delta f$. The costs are larger resolution cells by a factor B/b, and increased variance of the time delay. With SSA, the absolute phase at f_c becomes

$$\psi_a(f_c) = \frac{f_c}{\Delta f}\psi_a(\Delta f). \tag{8}$$

By inserting the variance for the time delay estimate of each subband $\sigma^2_{f_1}$ and $\sigma^2_{f_2}$ we find the corresponding variance on the estimate using the delta frequency $\sigma^2_{\Delta f}$ to be

$$\sigma^2_{\Delta f} = \frac{f_2\sigma^2_{f_2} + f_1\sigma^2_{f_1}}{f_2 - f_1}. \tag{9}$$

The Split-Spectrum Algorithm described in the literature uses only two subbands. Within this restriction it has been shown that the smallest variance is achieved by dividing the total bandwidth B into three equal parts and using the upper and lower bands [19]. The split spectrum technique uses the same principle as in ΔK, first exploited by [33] in radar applications.

C. Multi-Chromatic Approach (MCA)

An alternative method that can be used on either two or multiple frequency bands is the Multi-Chromatic Approach (MCA) [14], [34]. MCA, as with SSA, takes advantage of that the absolute phase difference is proportional to the frequency. The original master and slave images are divided into two or multiple bands at different center frequencies $f_n, n = 1, 2, 3, \ldots, N$ with reduced bandwidth $b < B$. Each subband can overlap in frequency domain $b > B/N$ [35], [36]. Interferograms at different center frequencies will wrap at different intervals. As a result, the time delay t_d can be estimated by comparing the wrap combinations for the different interferograms.

Functionally, the estimator can be described as follows. We construct a series of vectors

$$\mathbf{k} = [k_1, k_2, \ldots, k_N], \quad k_n = 0, \pm 1, \pm 2, \ldots \tag{10}$$

containing candidate solutions within certain limits given by geometry and baseline. We then form a cost function which is the variance of the absolute phase estimate for a given candidate $\mathbf{k}$

$$J(\mathbf{k}) = \frac{1}{N}\sum_{n=1}^{N}\left\{\frac{f_c}{f_n}\left(\psi_w(f_n) + 2\pi k_n\right) - \psi_{avg}(f_c, \mathbf{k})\right\}^2 \tag{11}$$

where

$$\psi_{avg}(f_c, \mathbf{k}) = \frac{1}{N}\sum_{n=1}^{N}\frac{f_c}{f_n}\left\{\psi_w(f_n) + 2\pi k_n\right\} \tag{12}$$

is the average absolute phase for the given selection of $\mathbf{k}$. We then minimize the cost function

$$\mathbf{k}_{min} = \arg\min_{\mathbf{k}} J(\mathbf{k}) \tag{13}$$

to determine the optimal choice of wraps per subband $\mathbf{k}_{min}$. The absolute phase difference is then estimated by averaging over all subbands

$$\psi_a(f_c) = \frac{1}{N}\sum_{n=1}^{N}\frac{f_c}{f_n}\left\{\psi_w(f_n) + 2\pi k_{n,min}\right\}. \tag{14}$$

In the general case of different variance in different bands, the above least squares method should be modified to incorporate weights of $1/\sigma^2$ [14], [20]. The multifrequency interferometry method [15], [21] give a result similar to MCA, but it approaches the problem thorough the PDF of the absolute phase estimate rather than through the error function of the absolute phase estimate.

D. Weighted Multiband Split-Spectrum Algorithm (WSSA)

In order to use all the signal information, we suggest an extension of SSA to multiple bands. As with MCA, we divide the signal bandwidth into N bands. We then form all the difference frequencies $\Delta f_{nm} = f_n - f_m$, using the description for SSA, where equation (9) is valid for non-overlapping subbands. There are $K = N(N-1)/2$ differences [37, chapter 3.3]. We estimate the absolute phase at f_c, $\psi_a(f_c)$, from the absolute phase of each band pair, $\psi_a(\Delta f_{nm})$, and average all to form a final estimate of the absolute phase difference

$$\psi_a(f_c) = \frac{1}{w_{tot}}\sum_{n=1}^{N}\sum_{\substack{m=1\\m\neq n}}^{n} w_{nm}\frac{f_c}{\Delta f_{nm}}\psi_a(\Delta f_{nm}). \tag{15}$$

w_{nm} is a weight that can be chosen, and w_{tot} is a normalization factor. By choosing $w_{nm} = 1/\sigma^2_{\Delta f_{nm}}$ from (9) and

$$w_{tot} = \frac{1}{\sigma^2_{\Delta f_{tot}}}, \quad \sigma^2_{\Delta f_{tot}} = \sum_{n=1}^{N}\sum_{\substack{m=1\\m\neq n}}^{n}\sigma^2_{\Delta f_{nm}} \tag{16}$$

we get a *weigthed multiband SSA* estimate, where the weights of the individual band-pairs are the inverse of the variance $1/\sigma^2_{\Delta f_{nm}}$. By using the actual estimates for $\sigma^2_{f_i}$, this is an adaptive filter that minimizes the variance of the combined absolute phase difference estimate. Such adaption to the data will potentially improve the performance compared to deterministic filters when the subband variance changes over the bands. A similar type of weighting was suggested for MCA in [14], [20]. By assuming the same variance for each subband, we get a non-adaptive multiband method with the (relative) weights $w_{nm} = (f_2 - f_1)/(f_2 + f_1)$.

E. Summary of Methods

CCC is maximum likelihood and should theoretically achieve a Fisher efficiency of one (the ratio of the CRLB to the variance of the estimator). According to [38] the Fisher efficiency for SSA is 0.75 for two densely spaced subbands of $b = B/2$, and 0.89 by using two maximally separated

Dette er en postprint-versjon / This is a postprint version.
DOI til publisert versjon / DOI to published version: 10.1109/TGRS.2013.2244900

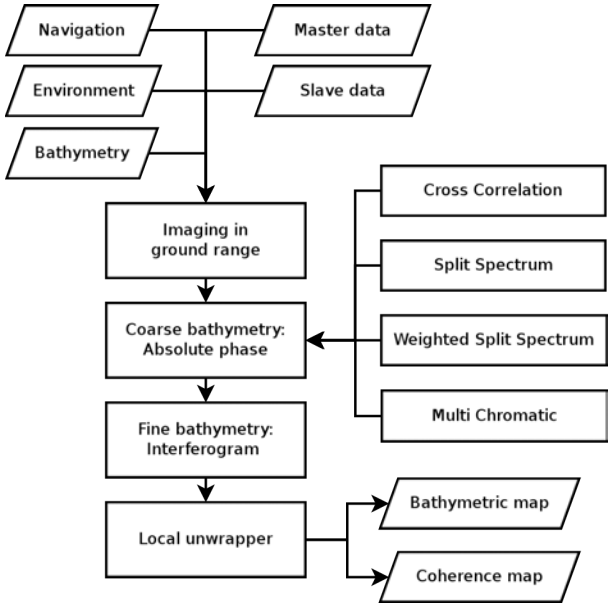

Fig. 5. Full wideband interferometry processing scheme including absolute phase difference estimation.

subbands of $b = B/3$. An extension of the method to four bands should give Fisher efficiencies of 0.93 and 0.96 respectively. Even so, our WSSA is an adaptive minimum least squares method that could outperform maximum likelihood estimators in the case of non-white noise.

Traditional narrowband SAR/SAS interferometry requires a 2D phase unwrapping stage (see Section II-C), where prior knowledge or specific properties of the data is assumed (smooth surfaces or such) [39]. Thus for narrowband systems, methods like Conditional Mean Estimate and Maximum A Posteriori (MAP) can obtain substantially higher performance than the MLE [40], when the prior knowledge is correct.

The key properties of the described methods are:

- CCC does a local coregistration, and always performs better than subband methods on misregistrated images.
- CCC is substantially slower than the other methods.
- MCA and multiband SSA have similar performance for the same choice of bands.
- Multiband SSA is simpler to implement and is faster than MCA for the same choice of bands.
- Multiband WSSA is always better than multiband SSA on the same choice of bands.
- Multiband SSA and MCA approaches the performance of CCC for large number of bands.

IV. Processing flow

Fig. 5 shows the basic processing flow for wideband SAS interferometry processing including the absolute phase estimation methods described in the previous section. In this section, we describe each of the components in this processing flow.

We first produce a master and a slave image which are coarsely coregistered by rendering the images on an *a priori* seafloor depth. The coarse registration is based on real aperture (or sidescan) seafloor depth estimation from the same data [41], [42]. The images are constructed using the backprojection algorithm, and are gridded in ground range. We pre-flatten the spectrum of the images as suggested in [35].

Then one of the absolute phase difference estimators are run to resolve the phase ambiguities of the full bandwidth interferogram. All of the methods use a maximum likelihood estimator to estimate the phase differences. In this article we have chosen to use a 9×9 pixels filter window. Since the images are slightly oversampled in 2×2 cm, the effective number of independent pixels in the phase difference estimators is approximately 50.

All the subband methods have increased variance compared to the variance of the phase difference on the full band interferogram (for CCC, the full bandwidth is incorporated in the estimation). We therefore only use the absolute phase difference estimates to determine the correct wrap

$$k(f_c) = \left\lfloor \frac{1}{2\pi} \left\{ \psi_a(f_c) - \psi_w(f_c) \right\} \right\rceil \tag{17}$$

where $\lfloor \rceil$ is the `round`-operator. In order to obtain the correct $k(f_c)$, each subband must be selected wide enough to yield a time delay estimate variance smaller than the wrap interval $1/f_c$.

In a standard interferogram, the phase differences are typically wrapped from smooth, continuous absolute phase differences. This may not be true for very complicated scenes. Thus large regions in the interferogram will have the same phase wraps, and a 2D phase unwrapper simply tries to connect the regions. After we have run one of the absolute phase difference estimators, the interferogram are in general unwrapped. However, there will remain small areas (with a size typical less then the phase difference estimation window) with incorrect wrap randomly distributed throughout the scene. As we saw in Fig. 4, the number of wrap errors is strongly dependent on the SNR. To remove these residual errors we have implemented a *local* unwrapper. The local unwrapper estimates the median value inside a small neighboring region and unwraps the phase difference to this value. This method removes the wrap errors provided that the number of incorrect wraps are significantly less than the number of correct wraps. The advantage with such a local method is that a small error in the method will not affect large regions in the unwrapped phase difference. Note that since the wrap errors are randomly located after we have run an absolute phase difference estimators, the data do now not fulfill the assumptions of most phase unwrappers. This means that running for example Goldsteins Branch algorithm on top of an absolute phase difference estimators will provide large errors.

V. Performance Assessment on Simulated Data

To test the performance we have simulated a scene consisting of a flat seafloor (simple) with a wreck (difficult). We have focused the SAS images onto a ground-plane with a 1 m depth error relative to the true depth of the flat part of the seafloor (which is realistic in real scenarios).

The simulated wreck has a height which is up to 4 m off the *a priori* depth. The simulated sonar is a HISAS 1030 sonar with 30 kHz bandwidth around 100 kHz center

Dette er en postprint-versjon / This is a postprint version.
DOI til publisert versjon / DOI to published version: 10.1109/TGRS.2013.2244900

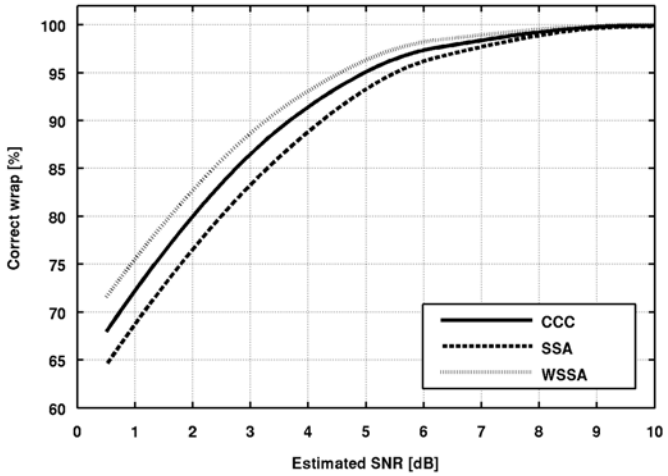

Fig. 6. Probability of correct wrap as a function of SNR for the different methods . For WSSA we have used five dense subbands and for SSA we have used two sparse subbands.

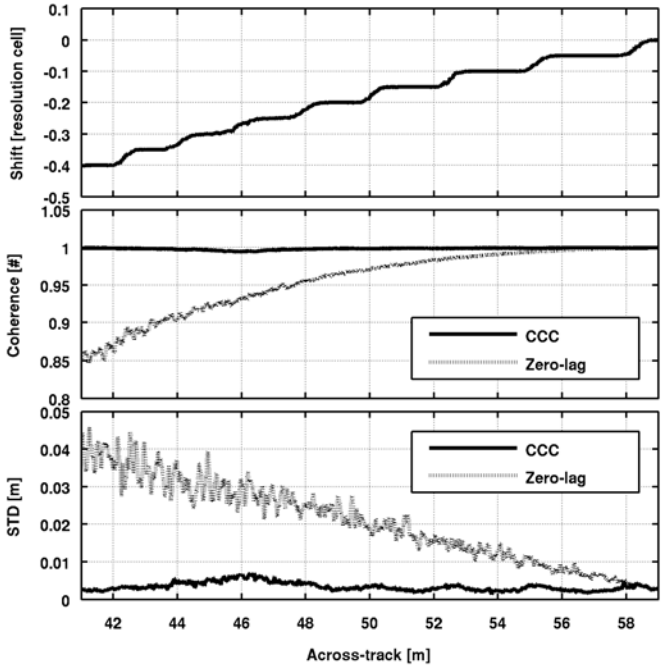

Fig. 7. Estimated across-track pixel shift (top), estimated coherence (center) and estimated standard deviation (bottom) as a function of across-track distance. The results are the average over 400 along-track lines in the flat region of our noise-free simulated data.

frequency, and a 30 cm vertical baseline ($20\,\lambda$). The wreck is at 10 meters water depth and the ground range in the simulation extends from 41 to 59 meters. The front of the wreck causes significant layover which causes problems for all of the considered methods. Recent work [43], [44] show promising results in reducing the effect of layover via the SAR tomography technique, but such methods are outside the scope of this paper.

In our implementation, we have found that MCA and multiband SSA have similar performance for the same choice of bands. We therefore only consider multiband SSA, WSSA and CCC here.

We have evaluated two performance measures:

A. Robustness

We study the robustness of the techniques by investigating how often the methods successfully manage to estimate the correct wrap. In this case we have considered the flat seafloor region of our simulation. The findings are: WSSA and SSA have similar performance on two subbands; WSSA is better than SSA for three or more subbands; more subbands are better; the number of subbands should be lower than the number of across-track pixels in the phase difference estimation window; when using two subbands these should be sparse; when using five subbands these should be densely spaced; CCC is better than WSSA and SSA up to three subbands, but WSSA and SSA with five subbands are better than CCC (see discussion below). In Fig. 6 we show the performance of the most relevant methods as a function of estimated SNR. Notice that the results in Fig. 6 only applies to this specific scenario and should only be used to compare the relative performance between the methods.

WSSA is an adaptive method that can outperform CCC. However, we found that multiband SSA also outperformed CCC, while we expected CCC to have the highest score of the none-adaptive methods. This could be a consequence of CCC being a higher order model. CCC estimates shift in addition to phase-difference, in contradiction to WSSA and SSA which assumes zero-lag. In this simulation the shift is only a small fraction of a resolution cell, so zero-lag is the correct answer. This mean that WSSA and SSA have *a priori* knowledge which CCC does not have.

B. Accuracy

We study the accuracy of the techniques by investigating the actual variance on the final depth estimates. CCC estimates a shift and perform better than the other methods if there is significant misregistration between the images. If we assume that the wrap is correct, both WSSA and SSA have the same accuracy as regular phase-differencing. This is because we only use WSSA and SSA to estimate the wraps and then we apply full bandwidth phase-differencing on top.

In Fig. 7 we show a comparison between the zero-lag methods and CCC. In the upper panel we show the estimated pixel shift from CCC. The steps in the shift are due to the finite sampling inside CCC. In the center panel we compare the estimated coherence between the the zero-lag methods and CCC. Notice the significant coherence loss which occurs when the shift is more than a twentieth of a resolution cell. Since we have simulated a system where the resolution is comparable to the wavelength, we observe significant coherence loss even below the usual coregistration demand of approximately a tenth of a resolution cell [10]. In the lower panel we show the corresponding standard deviation of the estimate. Note that all methods are unbiased. For a realistic SNR the curves would have been much closer, but the figure illustrates that for high SNR, any misregistration would cause coherence loss for the zero-lag methods.

Dette er en postprint-versjon / This is a postprint version.
DOI til publisert versjon / DOI to published version: 10.1109/TGRS.2013.2244900

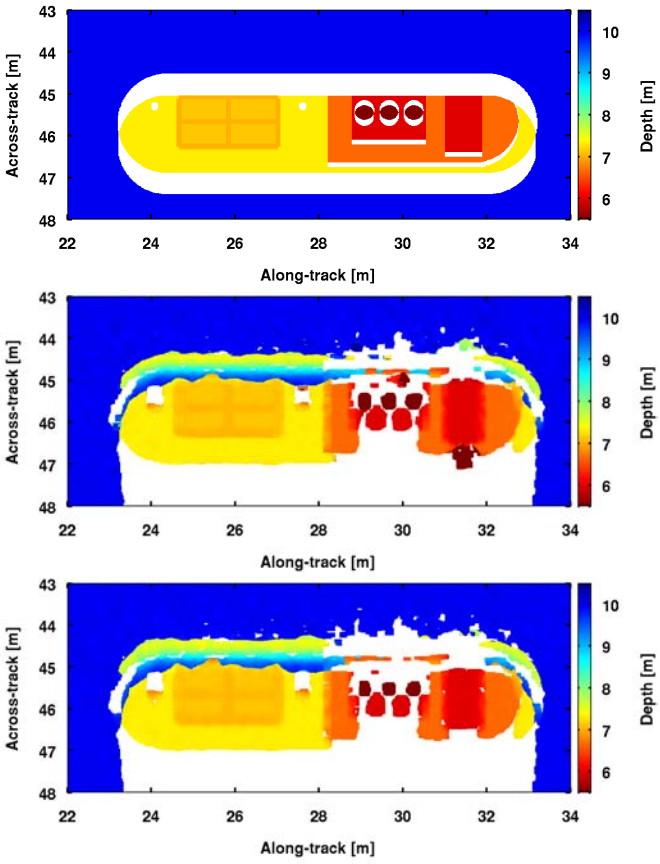

Fig. 8. Model bathymetry (top), CCC based bathymetry (center) and WSSA based bathymetry (bottom). In the model, both the layover region and the shadow region have been removed. In the center and lower panel all estimates with a coherence below 0.55 are removed. The average SNR in the SAS images are around 10 dB.

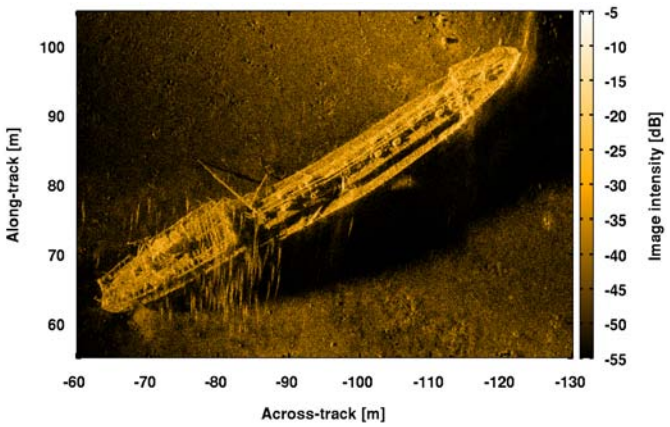

Fig. 9. SAS image of the wreck of the Holmengraa. Data courtesy of Kongsberg Maritime.

In Fig. 8 we show the simulated and estimated bathymetry on the simulated wreck. All the absolute phase difference estimators have very few wrap-errors, but they fail in the layover region (due to the overlap of responses from the wreck and seafloor). On the wreck, however, there is a significant shift in the interferometric images and therefore CCC performs best. For WSSA, we have used 5 dense subbands. We also tested the Goldstein's Branch cut algorithm, and it fails severely in reconstructing the depth of the wreck.

VI. Experimental Results

We have tested the wideband interferometry methods on real data collected with a HISAS 1030 interferometric SAS (see Fig. 1). The data were collected in February 2012, south of Horten, Norway, at approximately 77 m water depth. As for the simulated data, the experimental data are collected using 30 kHz bandwidth around 100 kHz center frequency, and with a 30 cm vertical baseline. The object of interest is the wreck of the 1500 dead weight tons oil tanker Holmengraa, that was sunk during World War II. The length of the wreck is 68 m, and the width is 9 m. Fig. 9 shows the SAS image of the wreck. The range to the center of the image is 95 m, and the image size is 50 x 80 m. The bright lines on top of the bridge in the lower left corner of the image, is a school of fish. The theoretical resolution in the image is around 3 x 3 cm, and the grid resolution is 2 x 2 cm. Fig. 10 shows CCC based coherence and interferogram. We see that the coherence is very high (red color) in the flat areas around the wreck, and on some parts of the wreck. In the shadow region, and over complex areas of the wreck, the coherence is low (blue color). The interferometric phase difference (lower panel) varies slowly over the seafloor surrounding the wreck. On the wreck, especially in the aft part, there are rapid variations and disconnected regions, which will cause difficulties for 2D phase unwrappers.

Fig. 11 and Fig. 12 show the wideband SAS interferometry results based on CCC, WSSA and Goldstein's Branch cut algorithm. We see that all three techniques are performing well on the seafloor around the wreck, and on the fore part of the wreck. On the bridge (the aft part), the Goldstein algorithm fails badly. WSSA performs satisfactory and produces plausible depth estimates of all parts of the wreck. CCC performs even better, having more valid measurements compared to WSSA due to the local coregistration. In addition, CCC also produces probable depth estimates of the school of fish (red stripes over the bridge of the wreck in the lower left corner). This part of the image has severe layover with a large elevated structure on the wreck and a school of fish on top.

The fish over the bridge are moving targets that move a large number of wavelengths during the synthetic aperture data acquisition. They therefore cause defocus [45, chapter 7] in the SAS image, and each fish mainly appear as a stripe along-track. Somewhat surprisingly, CCC coherence is high on the defocused fish. This is due to the fact that the defocus is approximately equal on the master and slave image, and high coherence is maintained.

VII. Conclusions

In this paper we have considered different techniques for estimating absolute phase difference in wideband synthetic aperture sonar interferometry. The benefit of using such techniques is that a 2D phase unwrapper where prior knowledge or specific properties of the data is assumed is not needed. The studied techniques are the complex cross correlation (CCC),

Dette er en postprint-versjon / This is a postprint version.
DOI til publisert versjon / DOI to published version: 10.1109/TGRS.2013.2244900

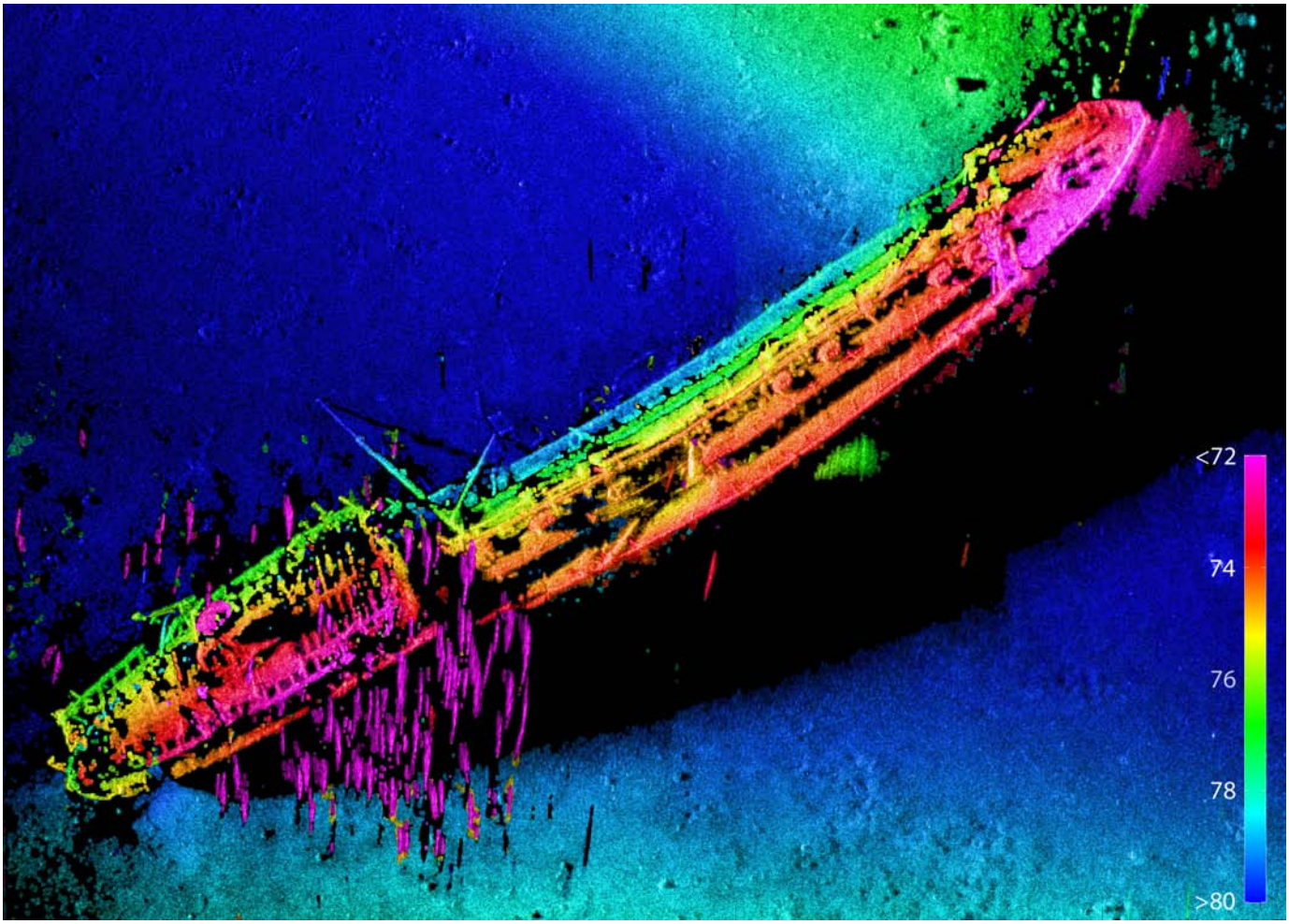

Fig. 11. Wideband SAS interferometry results based on a fusion of image, coherence and bathymetry of the image shown in Fig. 9. Depth is color coded, and brightness is based on image intensity and coherence. The colorbar shows depth in meters relative to the sloping imaging plane which is fitted to match the a-priori seafloor depth. The depth estimates are based on the CCC technique. Data courtesy of Kongsberg Maritime, Norway.

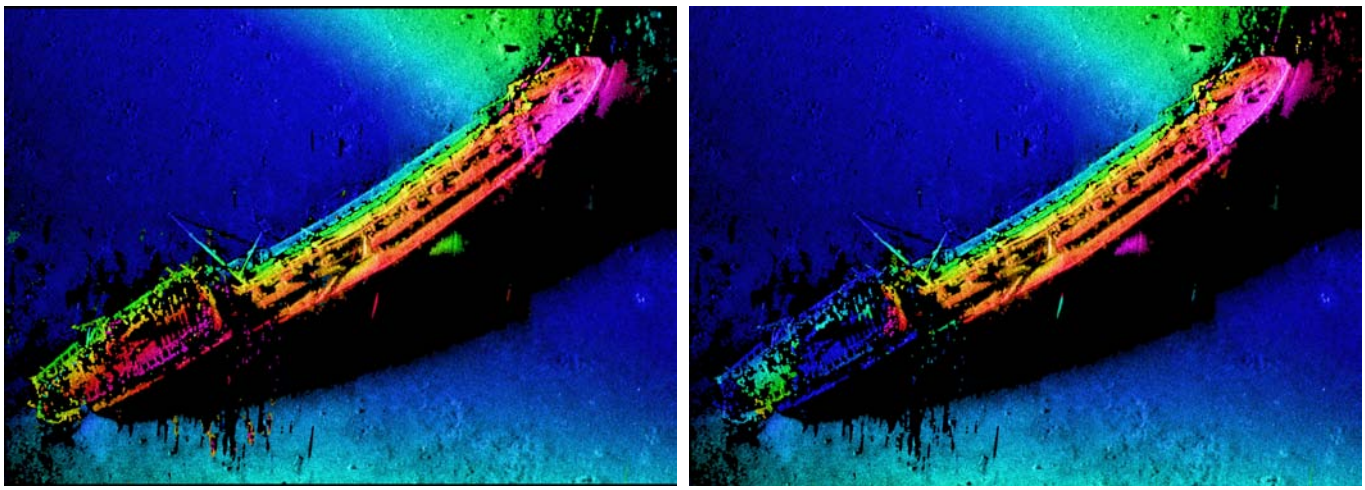

Fig. 12. Fusion of SAS image, coherence and bathymetry. Left: WSSA. Right: Goldstein‘s Branch cut algorithm. See Fig. 11 for comparison with CCC.

Dette er en postprint-versjon / This is a postprint version.
DOI til publisert versjon / DOI to published version: 10.1109/TGRS.2013.2244900

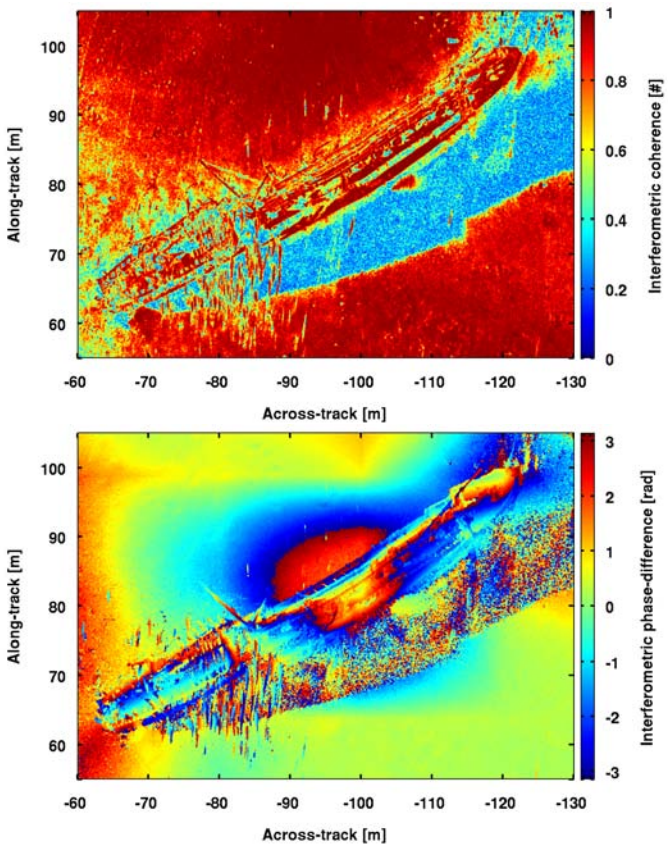

Fig. 10. Cross correlation based coherence (upper panel) and interferogram (lower panel) of the scene shown in Fig. 9.

the split-spectrum algorithm (SSA), the multi-chromatic approach (MCA), and the weighted split-spectrum algorithm (WSSA). We have benchmarked the techniques on a simulated scenario, and demonstrated the techniques on real data. WSSA obtained the best performance on the flat area while CCC obtained the best performance on complicated topographies. MCA has similar performance as multiband SSA for the same choice of subbands. In our implementation, multiband SSA is much faster than MCA. We have found that all four wideband interferometry techniques seems well suited for the HISAS wideband interferometric SAS, and they all outperform a standard Goldstein's Branch cut phase unwrapping algorithm on real data containing a complicated scene containing an elevated target and severe layover.

ACKNOWLEDGEMENTS

The authors thank Kongsberg Maritime for the kind permission to use data recorded with their HUGIN 1000 AUV. The authors also thank Hayden Callow at Kongsberg Maritime for fruitful discussions and valuable input.

REFERENCES

[1] M. P. Hayes and P. T. Gough, "Synthetic Aperture Sonar: A Review of Current Status," *IEEE J. Oceanic Eng.*, vol. 34, no. 3, pp. 207–224, July 2009.

[2] R. E. Hansen, "Introduction to Synthetic Aperture Sonar," in *Sonar Systems*, N. Z. Kolev, Ed. Intech, September 2011, ch. 1, pp. 3–28. [Online]. Available: http://www.intechopen.com/books/show/title/sonar-systems

[3] H. D. Griffiths, T. A. Rafik, Z. Meng, C. F. N. Cowan, H. Shafeeu, and D. K. Anthony, "Interferometric Synthetic Aperture Sonar for High-Resolution 3D Mapping of the Seabed," *IEE Proc. Radar, Sonar Navig.*, vol. 144, no. 2, pp. 96–103, April 1997.

[4] W. W. Bonifant Jr, M. A. Richards, and J. H. McClellan, "Interferometric height estimation of the seafloor via synthetic aperture sonar in the presence of motion errors," *IEE Proc. Radar, Sonar Navig.*, vol. 147, no. 6, pp. 322–330, December 2000.

[5] T. O. Sæbø, "Seafloor Depth Estimation by means of Interferometric Synthetic Aperture Sonar," Ph.D. dissertation, University of Tromsø, Norway, September 2010.

[6] H. D. Griffiths, "A comparison between radar and sonar synthetic aperture interferometry," in *IEE Colloquium on Radar Interferometry*, no. 153, 1997, pp. 4/1–4/5.

[7] T. O. Sæbø and R. E. Hansen, "Comparison between Interferometric SAS and Interferometric SAR," in *Proceedings of Synthetic Aperture Sonar and Radar 2010*, Lerici, Italy, September 2010.

[8] P. E. Hagen, T. G. Fossum, and R. E. Hansen, "HISAS 1030: The Next Generation Mine Hunting Sonar for AUVs," in *UDT Pacific 2008 Conference Proceedings*, Sydney, Australia, November 2008.

[9] T. G. Fossum, P. E. Hagen, B. Langli, and R. E. Hansen, "HISAS 1030: High resolution synthetic aperture sonar with bathymetric capabilities," in *Proceedings of Shallow survey*, Portsmouth, NH, USA, October 2008.

[10] R. F. Hanssen, *Radar Interferometry: Data Interpretation and Error Analysis*. Dordrecht, The Netherlands: Kluwer Academic Publishers, 2001.

[11] P. A. Rosen, S. Hensley, I. R. Joughin, F. K. Li, S. N. Madsen, E. Rodriguez, and R. M. Goldstein, "Synthetic Aperture Radar Interferometry," *Proc. IEEE*, vol. 88, no. 3, pp. 333–382, 2000.

[12] R. Bamler and P. Hartl, "Synthetic aperture radar interferometry," *Inverse Problems*, vol. 14, pp. R1–R54, 1998.

[13] R. Bamler and M. Eineder, "Split band interferometry versus absolute ranging with wideband SAR systems," in *Proceedings of IGARSS'04*, Anchorage, Alaska, September 2004.

[14] N. Veneziani, F. Bovenga, and A. Refice, "A wide-band approach to the absolute phase retrieval in SAR interferometry," *Multidimensional Systems and Signal Processing*, vol. 14, no. 1, pp. 183–205, 2003.

[15] V. Pascazio and G. Schirinzi, "Multifrequency InSAR height reconstruction through maximum likelihood estimation of local planes parameters," *IEEE Trans. Image Process.*, vol. 11, no. 12, pp. 1478–1489, December 2002.

[16] S. Madsen, "Absolute phase determination techniques in SAR interferometry," in *Proceedings of SPIE*, vol. 2487, 1995, p. 393.

[17] T. O. Sæbø, R. E. Hansen, and A. Hanssen, "Relative Height Estimation by Cross-correlating Ground-Range Synthetic Aperture Sonar Images," *IEEE J. Oceanic Eng.*, vol. 32, no. 4, pp. 971–982, October 2007.

[18] S. Madsen and H. Zebker, "Automated absolute phase retrieval in across-track interferometry," in *Proceedings of IGARSS'92*, Houston, Texas, May 1992.

[19] R. Bamler and M. Eineder, "Accuracy of differential shift estimation by correlation and split-bandwidth interferometry for wideband and delta-k SAR systems," *IEEE Geosci. Remote Sens. Lett.*, vol. 2, no. 2, pp. 151–155, 2005.

[20] N. Veneziani, F. Bovenga, F. Lovergine, and A. Refice, "A frequency domain differential approach to the absolute phase retrieval in SAR interferometry," in *Proceedings of IGARSS'00*, Honolulu, Hawaii, July 2000.

[21] V. Pascazio and G. Schirinzi, "Estimation of terrain elevation by multifrequency interferometric wide band SAR data ," *IEEE Signal Proc. Lett.*, vol. 8, no. 1, pp. 7–9, January 2001.

[22] J. C. V. Jakowatz, D. E. Wahl, P. H. Eichel, D. C. Ghiglia, and P. A. Thompson, *Spotlight-Mode Synthetic Aperture Radar: A Signal Processing Approach*. Dordrecht, The Netherlands: Kluwer Academic Publishers, 1996.

[23] G. Fornaro and G. Franceschetti, "Image registration in interferometric SAR processing," *IEE Proc. Radar, Sonar Navig.*, vol. 142, no. 6, pp. 313–320, December 1995.

[24] S.-H. Hong, H.-S. Jung, and J.-S. Won, "Extraction of ground control points (GCPs) from synthetic aperture radar images and SRTM DEM," *International Journal of Remote Sensing*, vol. 27, no. 18, pp. 3813–3829, 2006.

[25] D. C. Ghiglia and M. D. Pritt, *Two-Dimensional Phase Unwrapping: Theory, Algorithms, and Software*. John Wiley & Sons, INC, 1998.

[26] A. Weiss and E. Weinstein, "Fundamental limitations in passive time delay estimation–Part I: Narrow-band systems," *IEEE Trans. Acoust., Speech, Signal Process.*, vol. 31, no. 2, pp. 472–486, April 1983.
[27] E. Weinstein and A. Weiss, "Fundamental limitations in passive time-delay estimation–Part II: Wide-band systems," *IEEE Trans. Acoust., Speech, Signal Process.*, vol. 32, no. 5, pp. 1064–1078, October 1984.
[28] M. S. Seymour and I. G. Cumming, "Maximum Likelihood Estimation for SAR Interferometry," in *Proceedings of IGARSS'94*, vol. 4. Pasadena, California: IEEE, August 1994, pp. 2272–2275.
[29] S. M. Kay, *Fundamentals of Statistical Signal Processing: Estimation Theory*. Prentice Hall International Editions, 1993.
[30] L. M. H. Ulander and P.-O. Frölind, "Ultra-Wideband SAR Interferometry," *IEEE Trans. Geosci. Remote Sens.*, vol. 36, no. 5, pp. 1540–1550, September 1998.
[31] C. K. Knapp and G. C. Carter, "The Generalized Correlation Method for Estimation of Time Delay," *IEEE Trans. Acoust., Speech, Signal Process.*, vol. ASSP-24, no. 4, pp. 320–327, 1976.
[32] G. C. Carter, "Coherence and Time Delay Estimation," *Proc. IEEE*, vol. 75, no. 2, pp. 236–255, February 1987.
[33] T. Hagfors, "Some Properties of Radio Waves Reflected from the Moon and Their Relation to the Lunar Surface," *J. Geophys Res.*, vol. 66, no. 3, pp. 777–785, 1961.
[34] N. Veneziani and V. Giacovazzo, "A multi-chromatic approach to SAR interferometry: differential analysis of interferograms at close frequencies in the spatial domain and frequency domain," in *Proceedings of IGARSS'06*. IEEE, 2006, pp. 3723–3726.
[35] F. Bovenga, V. M. Giacovazzo, A. Refice, N. Veneziani, and R. Vitulli, "A first validation experiment for a Multi-Chromatic Analysis (MCA) of SAR data starting from SLC images," in *Proceedings of IGARSS'09*, Cape Town, South Africa, July 2009.
[36] F. Bovenga, V. Giacovazzo, A. Refice, N. Veneziani, D. Derauw, and R. Vitulli, "Interferometric multi-chromatic analysis of TerraSAR-X data," in *TerraSAR-X Science Team Meeting*, Oberpfaffenhofen, Germany, February 2011.
[37] D. H. Johnson and D. E. Dudgeon, *Array Signal Processing: Concepts and Techniques*, ser. Signal processing series. Englewood Cliffs, NJ, USA: Prentice Hall, 1993.
[38] R. Brcic, M. Eineder, and R. Bamler, "Interferometric absolute phase determination with TerraSAR-X wideband SAR data," in *Proceedings of IEEE Radar Conference 2009*, Pasadena, California, May 2009.
[39] G. Nico, G. Palubinskas, and M. Datcu, "Bayesian approaches to phase unwrapping: theoretical study," *IEEE Trans. Signal Process.*, vol. 48, no. 9, pp. 2545–2556, 2000.
[40] O. Loffeld, H. Nies, S. Knedlik, and Y. Wang, "Phase Unwrapping for SAR Interferometry - A Data Fusion Approach by Kalman Filtering," *IEEE Trans. Geosci. Remote Sens.*, vol. 46, no. 1, pp. 47–58, 2008.
[41] T. O. Sæbø and B. Langli, "Comparison of EM 3000 multibeam echo sounder and HISAS 1030 interferometric synthetic aperture sonar for seafloor mapping," in *Proceedings of European Conference on Underwater Acoustic (ECUA) 2010*, Istanbul, Turkey, July 2010, pp. 451–461.
[42] R. E. Hansen, H. J. Callow, T. O. Sæbø, and S. A. V. Synnes, "Challenges in Seafloor Imaging and Mapping with Synthetic Aperture Sonar," *IEEE Trans. Geosci. Remote Sens.*, vol. 49, no. 10, pp. 3677–3687, October 2011.
[43] A. Reigber and A. Moreira, "First Demonstration of Airborne SAR Tomography Using Multibaseline L-Band Data," *IEEE Trans. Geosci. Remote Sens.*, vol. 38, no. 5, pp. 2142–2152, September 2000.
[44] X. Zhu and R. Bamler, "Demonstration of Super-Resolution for Tomographic SAR Imaging in Urban Environment," *IEEE Trans. Geosci. Remote Sens.*, vol. 50, no. 8, pp. 3150–3157, August 2012.
[45] V. C. Chen and H. Ling, *Time-Frequency Transforms for Radar Imaging and Signal Analysis*. Boston, MA: Artech House, 2002.

Torstein Olsmo Sæbø (M'06) was born in Bergen, Norway, in 1977. He received the cand.scient. (M.Sc.) degree in astrophysics in 2002, from the University of Oslo, Norway. Since 2002, he has been working as a Scientist at the Norwegian Defence Research Establishment (FFI), Kjeller, Norway, specializing in the field of interferometry on synthetic aperture sonar. In 2010 he received the Ph.D degree in physics from the University of Tromsø, Norway, entitled *Seafloor Depth Estimation by means of Interferometric Synthetic Aperture Sonar*.

Stig Asle Vaksvik Synnes was born in Ålesund, Norway, in 1972. He received the Cand.Scient. (M.Sc.) degree in atomic physics from the University of Bergen, Norway, in 1997. Since 1998, he has been with the Norwegian Defence Research Establishment (FFI), Kjeller, Norway. His main research interests have been on perimeter surveillance systems, electromagnetic modeling, naval mine countermeasures and synthetic aperture sonar. SAS research include shallow water sonar performance and correlation based navigation. Currently he is working on a Ph.D in ultra wide-band SAS.

Roy Edgar Hansen (M'07) received the M.Sc. degree in physics in 1992, and the Ph.D. degree in physics in 1999, both from the University of Tromsø, Norway. From 1992 to 2000 he was with the Norwegian research company TRIAD, working on multistatic sonar, multistatic radar, SAR and underwater communications. Since 2000, he has been working at the Norwegian Defence Research Establishment (FFI), Kjeller, Norway. He is currently team-leader for the autonomous underwater vehicle development and the synthetic aperture sonar development at FFI. He is also adjunct associated professor at Centre for Imaging at University of Oslo, Norway.

Dette er en postprint-versjon / This is a postprint version.
DOI til publisert versjon / DOI to published version: 10.1109/TGRS.2013.2244900